Transverse Electromagnetic Fields in a Detuned X-Band Accelerating Structure

S. A. Kheifets, S. A. Heifets, and B. Woo

Abstract—Results are presented of a study of the dipole electromagnetic fields in a detuned accelerating section which are excited by a pointlike bunch. The field-matching technique is used for the field calculations. The transverse coupling impedance, the kick factors, and the point wake function are found.

I. INTRODUCTION

THE EM fields generated by the beam of particles in an accelerating structure, known as a wakefield, affects the beam stability. To avoid the build-up of the transverse wake field along the linear accelerator, it was suggested to use the detuned accelerating section [1] with slightly different (detuned) frequencies of individual cells. If the frequencies of the cells are distributed in a certain pattern—in particular, for the Gaussian distribution—the undesirable effects of the transverse fields are reduced substantially. This has been previously shown by approximating the structure with a chain of coupled equivalent circuits [2]. The parameters of the equivalent circuits have been obtained using numerical codes for periodic structures built out of different cells of the detuned section. For the Gaussian detuning (i.e., for the Gaussian distribution of the dipole field frequencies) with sigma $\approx 2.5\%$, the transverse wakefield acting on a bunch travelling at the distance of 40 cm behind the previous one has been shown to be reduced by a factor of ≈ 100. The high value of the reduction factor demands its accurate evaluation by other independent methods.

Here we present the results of a study of the deflecting dipole ($m = 1$) electromagnetic (EM) fields for the same structure excited by a pointlike charge, using computer code *PROGON* [3]. The code is based on the field-matching technique for the Fourier harmonics of the EM travelling waves. The calculation of the longitudinal monopole ($m = 0$) EM fields in that structure, including discussion of the choice of suitable couplers, can be found in [4], [5]. The geometry of the considered section—built out of 204 cells ($N_c = 204$)—can be found in [3].

The present paper consists basically of two parts.

In the first part (Section II), the results of calculation of the deflecting EM fields are presented for a detuned accelerating section.

For an infinitely periodic structure built out of connected rf cavities (cells), each eigenmode of a single cavity produces a passband with the continuum of allowed frequencies. Examples of dispersion curves are given for three different cells taken from the beginning, the middle, and the end of the accelerator section.

For an aperiodic structure, the concept of the passband has little meaning. But loosely, we will call a passband for the whole structure the passband of one of the cells that is the widest in the frequency domain.

For an accelerating section consisting of a finite number of cells, its passband splits into an equal number of the EM field modes. These modes are found in the whole range of frequencies corresponding to the first passband of the accelerating section. For each mode, including the trapped ones, the field pattern, the group velocity, and the stored energy are calculated. The dipole coupling impedance is then found in this range of frequencies. The computer time needed to calculate all these quantities for the considered detuned section consisting of 204 cells (a cell is a cavity and the adjacent iris) is approximately 15 minutes on the workstation *IBM RISC 6000*. In these calculations, 16 space harmonics in the cavity region, and 30 space harmonics in the iris region are taken into account.

The second part of this paper (Sections III and IV) is devoted to discussion of several different ways for evaluating the kick factors and the corresponding wake function. For a large number of cells, the transverse coupling impedance is represented by a large number of narrow interfering resonances. Under such conditions, the choice of the most accurate method to derive the wake function from the transverse coupling impedance, which is found numerically in a given finite number of frequency points, is a nontrivial problem.

A number of different authors have used the field-matching technique to obtain some of these results on various levels of development [6]–[8]. As we discussed in Section V, our results match most of their results quite well. Two computer programs, *TBCI* [9] and *ABCI* [10], are available which allow calculation of the wake function directly in the time domain. Unfortunately, due to limitations in achievable resolution, these programs are not suitable for calculations of the wake function for long and complex structures at a large distance behind the bunch.

Throughout the paper, the Gaussian system of units is used in which both electric $\vec{E}$ and magnetic $\vec{H}$ fields have the same dimensions.
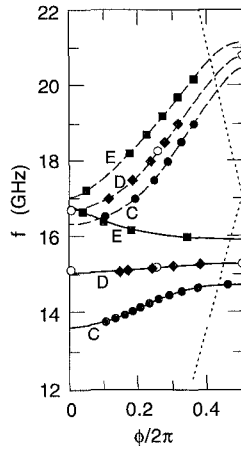
Fig. 1. The dispersion diagrams, reproduced from [2], for three periodic structures, labeled C, D and E, built of cells with geometries listed in Table I. The solid curves show the dispersion curves obtained by the program *TRANSVRS* for the first dipole passband, and the dashed curves show the same for the second dipole passband. The symbols give the results of calculations using the codes *PROGON* (full circle for cell type C, diamond for cell type D, and square for cell type E) and *URMEL* (open circle). The dotted lines correspond to velocity of light c.

II. DISPERSION CURVES, ELECTROMAGNETIC FIELDS, AND COUPLING IMPEDANCE

We first demonstrate the validity of the program *PROGON* by calculating the dispersion curves for an infinitely periodic structure corresponding to the three different geometries of the cells of the structure. They are labeled C for the cell at the beginning of the section, D for the cell in its middle, and E for the cell at its end. To facilitate the comparison, their labels and geometry are chosen to coincide with the labels and geometry considered in [2]. Let f be the frequency and ϕ the phase advance per cell of a periodic structure. The iris and cavity radii, and the synchronous f_s frequencies for the first and second passbands for the cells C, D and E, are given in Table 1. In Fig. 1 the solid curves labeled C, D, and E that are reproduced from [2] show the functions $f(\phi)$ obtained by the program *TRANSVRS* [11] for the first dipole passband, and the dashed curves [2] show the same for the second dipole passband. The symbols in Fig. 1 give the results of calculation using the codes *PROGON* (full symbols) and *URMEL* [12] (open circles). In this example, the matrices are truncated at 16 radial modes in a cavity and 30 modes in an iris. *PROGON* is in good agreement with both *TRANSVRS* and *URMEL*. Notice that there is a positive derivative of the dispersion curve C and a negative derivative of the dispersion curve E in the first passband. Since $df/d\phi$ is proportional to the group velocity, this is a necessary condition for the mode trapping.

A. Mode Patterns

Next, we illustrate the pattern of the EM field excited by a charge for three different frequencies that correspond to the excitation of the field in the beginning, middle, and end of the accelerating section. The purpose of Fig. 2 is to show localization of the mode at these different frequencies. The y-axis labels in Fig. 2 are not missing, they are irrelevant and are therefore arbitrary—the vertical scale does not matter, as long
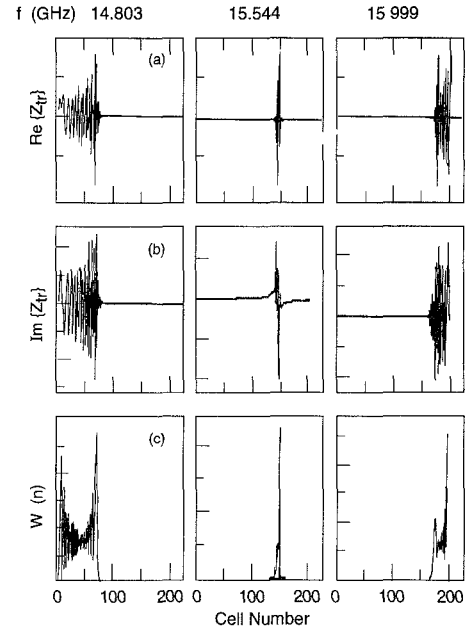

Fig. 2. Three examples of the field pattern in the detuned structure showing the mode trapping (in arbitrary units). For each frequency shown at the top of the plot the row label means: (a) the real part of the transverse impedance $\mathrm{Re}\{Z_{tr}(n)\}$; (b) the imaginary part of the transverse impedance $\mathrm{Im}\{Z_{tr}(n)\}$; (c) the stored electric $W_E(n)$ and magnetic $W_M(n)$ energy in the nth cell (both curves coincide).

TABLE I
CELL GEOMETRIES FOR THE THREE PERIODIC STRUCTURES IN Fig. 1. ALL CELLS HAVE IRIS THICKNESS $l = 0.146$ cm, GAP LENGTH $g = 0.729$ cm, AND PERIOD LENGTH $d = 0.875$ cm

Label	a (cm)	b (cm)	$f s1$ (GHz)	$f s2$ (GHz)
C	0.5250	1.112	14.80	19.89
D	0 4625	1.083	15.34	20.26
E	0.4000	1.058	15.97	20.68

as it is kept unchanged along the section. In Fig. 2, in panels a and b, respectively, the real and imaginary parts of the average synchronous component of the transverse EM force, i.e., the dipole coupling impedance Z_{tr}, see (1), are plotted for each frequency versus the cell number. The trapping of the field is exhibited for the frequencies which roughly correspond to the range 14.80 GHz < f < 15.97 GHz; cf., Table I.

B. Stored Energy and Group Velocity

After the EM fields in the structure are found, the corresponding stored energy $W(n) = W_E(n) + W_M(n)$ in the nth cell and the power flow $S_z(n)$ through the cavity cross section are found. These quantities define the relative group velocity $v_g(n)/c = S_z d/W$, where d is the cell length. The curves of the stored energy are plotted in panel c of Fig. 2 for each cell of the section, for the electric $W_E(n)$ and magnetic $W_M(n)$ stored energy separately. The two quantities are equal with high accuracy, and are indistinguishable in Fig. 2. ($W_E = W_M$ is an identity. It is exactly for this reason that the relation *can* be used to check the results of calculations, because if incorrect it will indicate an error in computation.) This is one of several checks performed to

ensure that the fields are caclculated correctly. Another such check is to demonstrate that the calculated EM fields satisfy boundary and continuity conditions at each boundary between cavities and irises. For the (standing) trapped modes, the power flow S_z and, correspondingly, the group velocity are zero. This is confirmed by direct calculations.

C. Coupling Impedance

The dipole transverse coupling impedance Z_{tr} is defined as integral of the transverse force from the dipole field excited by a charge Ne with offset r_0 acting on a test particle at the observation point z, r [13]

$$Z_{tr}(f) = -\frac{i}{eNr_0\cos\theta}\sum_{n=1}^{N_c}\int_0^d dz\, e^{ikz}[E_r(z,r) - H_\theta(z,r)].$$
(1)

Here k is the wave number $k = 2\pi f/c$. Each term in the sum is represented by a sum of two integrals—one in which the integration is performed over a cavity gap of length g, and the other over an iris of thickness l, $d = g + l$. In each such integral, the integration of the $E_r - H_\theta$ can be substituted by an integration of the derivative over r of the longitudinal component of the electric field E_z, using the identity which follows from the Maxwell equations for an axial symmetric structure. For example, the identity for a cavity is

$$ik\int_0^g dze^{-ikz}[E_r(z,r) - H_\theta(z,r)]$$

$$= \int_0^g dze^{-ikz}\frac{dE_z(z,r)}{dr} + E_r(0,r) - E_r(g,r)e^{-ikg}.$$
(2)

In the case when the last two terms in this identity are absent or cancel each other, (2) is the manifestation of the Panofsky-Wenzel theorem [14]. Expressions (1) and (2) are independent of the observation radius r, when it satisfies the condition $0 \le r \le b$ [15].

The main contribution to the impedance comes from the modes that are localized inside the section. For most of them, the field extensions to the entrance and to the exit of the section are small, and hence, for the perfectly conductive walls, the energy loss is very small. In this case, the real part of the impedance is represented by a series of extremely narrow peaks. The frequency position of each of them is difficult to find numerically, and it is even more difficult to evaluate the area under a peak with any reasonable accuracy.

This difficulty can be alleviated by taking into account a small energy loss either by considering a finite conductive wall of the section or by filling the section with a lossy dielectric. In the first approach, rather complicated boundary conditions need to be considered. We choose the second approach. The expressions for the field expansion in an axially symmetric structure filled with a dielectric that has a constant complex permittivity ϵ is given in the Appendix.

In the presence of such a dielectric, each resonance peak decreases in height and becomes wider, preserving the area under the peak. In this case, the heights and widths of the resonance peaks have no relation to the actual loss of the EM energy. Nevertheless, all the relevant physical quantities, such

as kick factors and wake functions, are expressed as integrals of the impedance and do not depend on the assumed imaginary part of the permittivity γ. This was confirmed numerically by showing that the area under the peaks is the same for different values of γ. A note of caution should be made in respect to the widths of the resonances. We discuss this problem below in Section IV.

At the same time, the choice of γ influences the choice of the frequency step size in the impedance calculations. Small γ decreases the needed frequency step and increases the time needed for accurate calculation of the impedance. If γ is chosen too big, the resonance peaks may strongly overlap. This would decrease the accuracy of the evaluation of the kick factors. As a reasonable compromise, we choose the permittivity to be $\epsilon = 1 + 0.5 \cdot 10^{-4}i$ and the frequency step 0.5 MHz. The sign of the imaginary part γ of the permittivity is chosen so that it will result in the energy dissipation (the sign of γ depends on the convention of the Fourier expansion of the fields).

The real and imaginary parts of the transverse coupling impedance $Z_{tr}(f)$ for the first dipole passband are presented in Fig. 3(a) and (b). The impedance is represented by a series of sharp peaks. In the middle of the passband they are separated from each other by ≈ 6 MHz. By an order of magnitude this number is the width of the passband divided by the number of cells: $(f_{s1E} - f_{s1C})/N_c$ (cf., Table I). The peak separation increases toward the edges of the passband.

III. KICK FACTORS

The analytic properties of the coupling impedance of any structure are defined by its poles and cuts in the complex plane of the variable $\omega = f/2\pi$. In the lowest passbands, the most important part of the impedance is given by a sum over poles, while the contribution of the cuts can be neglected. If the energy loss in the structure is small in comparison to the energy stored in the EM field, the shift of a pole from the real axis is small in comparison to its real value. Each pole produces a resonance peak in the impedance. The interference of the neighboring resonances generates an offset of the impedance curve. Hence, the calculated impedance including the offset may be approximated by a sum of the resonance terms.

A. Approximation of Impedance as a Sum of the Resonance Terms

The rth resonance peak in the calculated transverse impedance $Z_{tr}(f)$ can be approximated by

$$Z_{approx}^r(f) = i\kappa_r^{BW}\left(\frac{1}{f - f_r + i\Gamma_r} - \frac{1}{f + f_r + i\Gamma_r}\right).$$
(3)

Expression (3) with real resonance parameters κ_r^{BW}, f_r and Γ_r has the well known [16], [17] symmetry property of the transverse impedance $Z(-f) = -Z^\star(f)$, where the star means the complex conjugate value.

The offset in Z_{tr} should be taken out before a peak can be approximated by the resonance curve. After that, the resonance parameters for each resonance peak may be found, provided
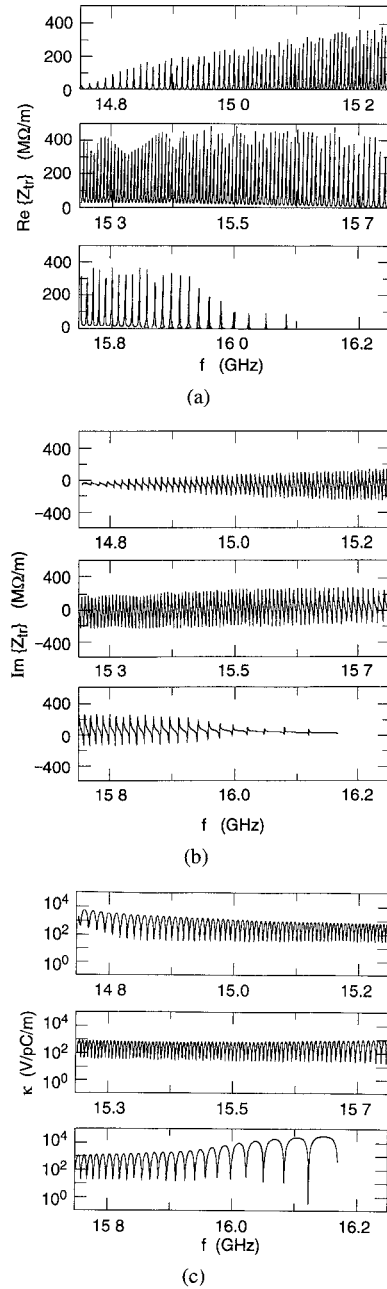
(a)

(b)

(c)

Fig. 3. (a) The real part of the transverse coupling impedance $\mathrm{Re}\{Z_{\mathrm{tr}}(f)\}$ for the first passband. (b) The imaginary part of the transverse coupling impedance $\mathrm{Im}\{Z_{\mathrm{tr}}(f)\}$ for the first passband. (c) The kick function $\kappa(f)$ obtained by formula (6) for the first passband.

that the impedance is calculated for a sufficiently large number of frequency points.

Panel a in Fig. 4 illustrates the procedure. The whole frequency range was split into intervals between the subsequent two minima of the calculated function $\mathrm{Re}\, Z_{\mathrm{tr}}(f)$ (represented by the curve going through the open circles in Fig. 4). Let the frequencies of the minima on both sides of the rth peak in $\mathrm{Re}\, Z_{\mathrm{tr}}$ be f_{1r} and f_{2r}. Then the difference $\mathrm{Re}\, Z_{\mathrm{tr}}(f) - \min[\mathrm{Re}\, Z_{\mathrm{tr}}(f_{1r}), \mathrm{Re}\, Z_{\mathrm{tr}}(f_{2r})]$, represented by the curve going through the full circles in Fig. 4, in the interval $f_{1r} \leq f \leq f_{2r}$ was approximated by the real part of the resonance function (3) using the least square method to find
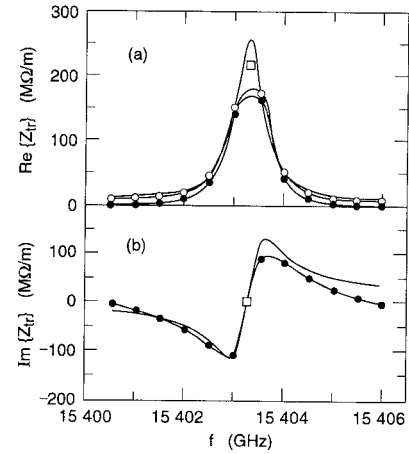

Fig. 4. Illustration of the approximation of one of the impedance peaks by the resonance curve (3). The resonance parameters found for this peak are: $\kappa^{BW} = 497.49$ V/pC/m, $\Gamma = 0.31952 \cdot 10^{-3}$ GHz, the resonance frequency $f = 15.403$ GHz, the vertical offset = 10.547 MΩ/m. The value of the impedance in the vicinity of the maximum of curve $\mathrm{Re}\, Z_{\mathrm{approx}}$ (open square) is calculated independently by $PROGON$. It is added after the least-square calculation is performed in order to illustrate the accuracy of the approximation.

the parameters κ_r^{BW}, f_r, and Γ_r. The real part of Z_{approx}^r for these parameters is shown without symbols in panel a of Fig. 4. The imaginary part of Z_{approx}^r (the curve without symbols) is compared with $\mathrm{Im}\, Z_{\mathrm{tr}}$ (represented by a curve going through full circles) in panel b of Fig. 4.

When the parameters of the resonance Z_{approx}^r for all the resonance peaks in the calculated impedance are found, the sum of the resonance terms $\sum_r Z_{\mathrm{approx}}^r$ represents a rather good approximation for the calculated impedance $Z_{\mathrm{tr}}(f)$, including the offset of its real part. The approximation is slightly worse toward the edges of the passband.

B. Various Methods to Evaluate Kick Factors

Given the transverse impedance, there are several ways to derive the kick factors κ_r. Each of the methods has its own advantages and drawbacks:

Method 1: If one approximates the calculated impedance $Z_{\mathrm{tr}}(f)$ by the sum of the resonance terms, (3), the parameter κ_r^{BW} is an estimate of the kick factor for the rth resonance at frequency f_r. The parameter Γ_r is inversely proportional to the quality factor Q_r of the rth resonance: $Q_r = f_r/2\Gamma_r$. The accuracy of such an estimate decreases at both edges of the passband, since the peaks of $Z_{\mathrm{tr}}(f)$ deviate there from the resonance shape. In this case, the least square method does not give an accurate evaluation of the kick factor. The magnitude of the kick factors at the edge of the passband is smaller then in its interior, but their distribution in frequency affects the behavior of the wake function at large distances.

Method 2: The kick factor $\kappa_r^{\mathrm{integ}}$ for the rth resonance can also be estimated by integration of the real part of the impedance $\mathrm{Re}\, Z_{\mathrm{tr}}^r$ between points f_{1r} and f_{2r}

$$\kappa_r^{\mathrm{integ}} = 2 \int_{f_{1r}}^{f_{2r}} df \mathrm{Re}\, Z_{\mathrm{tr}}^r(f). \qquad (4)$$

Notice that this formula, derived from (3), would be exact if there were only one resonance peak and $f_{2r} = \infty$, $f_{1r} = -\infty$. When there are many resonances, (4) does not take into account the effect of the peaks overlapping. As the consequence, the evaluation of the kick factor using this formula is reliable when the overlapping of the peaks is small.

Method 3: The kick factor can also be derived directly if the dipole EM field $E_z(z, r)$ is known. Define the voltage

$$V(r) = \int_0^L dz\, e^{-ikz} E_z(z, r) \tag{5}$$

where L is the total length of the section. Then calculate function

$$\kappa(f) = \frac{[V^\star(r_0)/r_0]dV(r)/dr}{4kW} \tag{6}$$

where W is the total stored energy for whole section $W = \Sigma_n W(n)$. Function $\kappa(f)$ can be calculated at the same time the impedance is calculated. Fig. 3(c) presents this function.

Strictly speaking, formula (6) has been derived [16, 17] to give the kick factor for a standing eigenmode of a closed cavity (with a descrite spectrum). The EM modes we are dealing with exist in an open section with attached infinite beam pipes. In the presence of the energy loss, the EM field has a continuous spectrum, and there is uncertainty in choosing a proper mode frequency. Nevertheless, it can be shown that this formula gives an approximation to the kick factor κ_r for the rth mode if it is evaluated at $f = f_r$; i.e., in the vicinity of the rth maxima of the real part of the transverse impedance. Hence, the kick factors κ_r^{WB} can be found by picking up the values of the function $\kappa(f)$ from (6) at $f = f_r$.

Fig. 5 illustrates an application of our main results. (The discrepancy in the kick factors obtained by different methods is a problem of these methods. In addition, both Figs. 5 and 7 illustrate the fact that calculations of the long range wakefields are sensitive to the subtle details, such as exact pattern of detuning or losses in the structure.) In Fig. 5, the kick factors obtained in three different ways are plotted as functions of frequency. For a comparison, we reproduce on the same plots the curve obtained using the equivalent circuit model [2]. The agreement in the two last cases is quite good, while the first method of obtaining the kick factor is not satisfactory. Agreement might be even better if the end conditions in both approaches were the same. (The structure considered in this paper has open ends, unlike the one with closed ends that was considered by Bane and Gluckstern [2].)

IV. WAKE FUNCTION

The point wake function [13] can be found by using its definition as the Fourier image of the coupling impedance.

A. Method 1

When the transverse impedance can be represented by the sum of the resonance terms, the point wake function

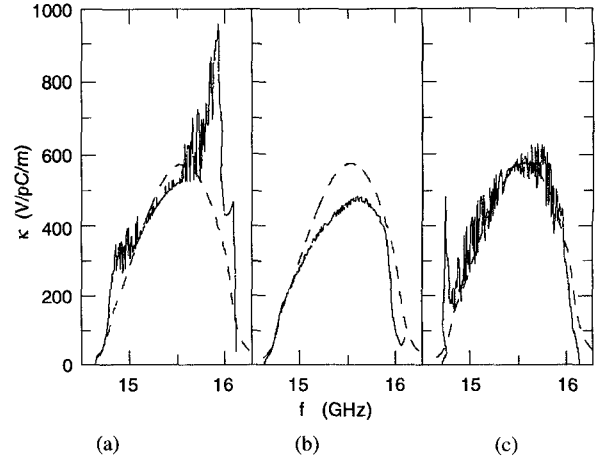$$w_{tr}(s) = -i \int_{-\infty}^\infty df\, e^{-iks} \sum_r Z_{approx}^r(f) \tag{7}$$

Fig. 5. Kick factors κ_r obtained in three different ways (solid curves): (a) Interpolation of the peaks by the resonance formula, (3); (b) integration of the real parts of Z_{tr}, (4); (c) the values of the function $\kappa(f)$ according to (6) at $f = f_r$ (see text). The results obtained by the equivalent circuit model [2] is presented for comparison (dashed curves, courtesy of K. Bane).

is expressed in terms of the resonance parameters κ_r, f_r, and Γ_r

$$w_{tr}(s) = \begin{cases} \sum_r \kappa_r e^{-2\pi\Gamma_r s/c} \sin 2\pi f_r s/c & s \geq 0, \\ 0 & s < 0. \end{cases} \tag{8}$$

Notice that in this case the causality ($w_{tr}(s) = 0$ for $s < 0$) is fulfilled automatically.

Now we can return to the problem of the widths of the resonance peaks Γ_r, which enter the expression (8) directly and influence the magnitude of the wake function at a very large distance behind the bunch. In practice, such a distance for a detuned accelerating section is much larger then the length of the bunch train, ≈ 40 m in our case. Indeed, for the considered number of cells, the summation in (8) can be substituted by an integration [2]. (The distance S for such a substitution to be valid should be smaller than $c/\Delta f$, where $\Delta f \approx 6$ MHz is frequency difference between neighboring resonances; i.e., $S < 50$ m). The result of integration can then be represented as a product of two exponential factors: one coming from the relative frequency spread $\sigma/f \approx 2.5\%$, and the other from the field damping $Q = f/2\Gamma$. Evaluating the Q-factor for which the damping could overcome the frequency spread, we get $Q < f/\sigma \approx 40$. The situation can be further improved by using the experimental or empirical values for the Q-factors in (8).

B. Method 2

On the other hand, if the impedance is known in the whole frequency range, the point wake function can be obtained by direct integration of the impedance, avoiding the necessity of evaluating the kick factors altogether

$$w_{tr}(s) = 2 \int_0^\infty df\, [\text{Im}Z_{tr} \cdot \cos ks - \text{Re}Z_{tr} \cdot \sin ks]. \tag{9}$$

In this case, it follows from the causality that for $s < 0$

$$\int_0^\infty df\, \text{Im}\, Z_{tr} \cdot \cos ks = \int_0^\infty df\, \text{Re}\, Z_{tr} \cdot \sin ks \tag{10}$$
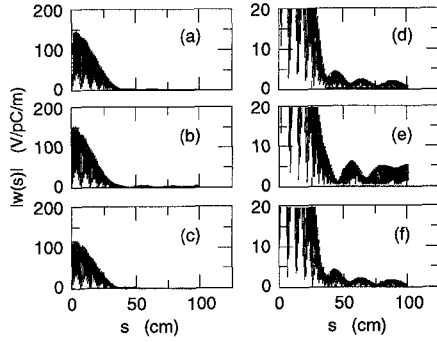
Fig. 6. The absolute values of the short-range wake function calculated in three different ways: panels (a, d) using direct integration of Z_{tr}, (11); panels (b, e) using (8) with the kicks calculated from (6); panels (c, f) using (8) with the kicks calculated from (4). In panels d, e, f, the same functions are plotted on a scale ten times larger for the vertical axis then in panels a, b, c, respectively, to show the reduction of the wake function.
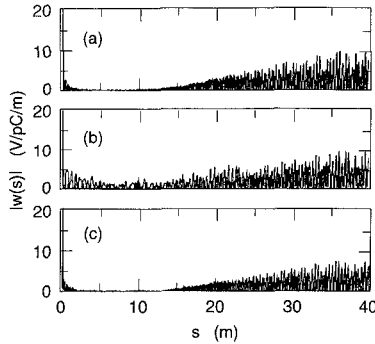

Fig. 7. The absolute values of the long-range wake function calculated in three different ways: panel (a) using direct integration of Z_{tr}, (11); panel (b) using (8) with the kicks calculated from (6), panel (c) using (8) with the kicks calculated from (4). Notice that the scale for the vertical axis is enlarged to show the growth of the wake function at large distances.

or

$$w_{tr}(s) = 4 \int_0^\infty df \, \text{Im} \, Z_{tr} \cdot \cos ks. \qquad (11)$$

Equation (10) can be employed as a control of the correctness of calculations.

In practice, the impedance can be calculated in a finite frequency range. Then formula (11) is applicable only when the impedance at high frequencies decreases rapidly enough. In each particular case, the range is determined by the contributions of higher passbands.

Fig. 6 gives the short-range point wake function calculated in three different ways, taking into account the impedance of the first passband only. The long-range wake is represented in Fig. 7. Apparent discrepancies shown in Fig. 7 (and Fig. 5) reflect the fact that calculations of the long range wake fields are sensitive to the subtle details, such as exact pattern of detuning or losses in the structure.

V. CONCLUSION

The results obtained by using the program *PROGON*, which is based on the field-matching technique, is in good agreement with the results obtained by means of other codes. In particular, the dispersion curves obtained here agree with those obtained

by the code *TRANSVRS*. The transverse coupling impedance agrees with that obtained in [8]. We compare different methods of obtaining the kick factors and find the two methods where the results are in good agreement with these obtained by the equivalent circuit method [2].

Nevertheless, the detailed behavior of the wake function is somewhat different for different methods of its calculations. Moreover, the most significant parameter—the magnitude of the wake function reduction for the subsequent bunches—has rather different values for different methods of its calculation. It well may be that the method of calculating the transverse wake function by directly integrating the transverse inpedance, (11), which avoids the calculation of the kick factors altogether, is the most accurate. In this case, indeed, the deflecting field acting on a bunch travelling at the distance of ≈ 40 cm behind the previous one is reduced by a factor of ≈ 100, as has been found in [2]; see Fig. 6(e). Further study is needed to ensure reliable results for this quantity.

For evaluation of the wake function, the coupling impedance is needed in an infinite range of frequencies. In other words, the accuracy of the evaluation depends on the amount of the contribution from the higher passbands of the section. In particular, the values of the impedance in the second passband are two orders of magnitude smaller then the impedance in the first passband. On the other hand, the obtained reduction factor is also of the same order of magnitude. Hence, inclusion of the effects of the higher passbands may be important.

APPENDIX

This appendix gives expressions for the Fourier components of the EM dipole $(m = 1)$ fields in the axially symmetric structure of the radius b, filled by a dielectric with a complex constant permittivity ϵ.

Suppose that a charge Ne moves with the velocity of light c along a line parallel to the axis of the structure at distance r_0. The EM field in the structure is the sum of the field of the charge and the radiation field excited by it. The expressions for the Fourier components at frequency f (and corresponding wave number $k = 2 \pi f/c$) of the total fields in the region $r > r_0$ are

$$\frac{E_r}{\cos\theta} = \frac{q}{\epsilon}e^{ikz}\left(\frac{1}{r^2} + \frac{1}{b^2}\right)$$
$$+ \sum_{l=1}^\infty \left[\lambda_l \frac{dJ_1(\nu_l r/b)}{dr}y_l(z) - k\frac{J_1(\mu_l r/b)}{r}\tilde{y}_l(z)\right],$$
$$\qquad (A1)$$

$$\frac{E_\theta}{\sin\theta} = \frac{q}{\epsilon}e^{ikz}\left(\frac{1}{r^2} - \frac{1}{b^2}\right)$$
$$- \sum_{l=1}^\infty \left[\lambda_l \frac{J_1(\nu_l r/b)}{r}y_l(z) - k\frac{dJ_1(\mu_l r/b)}{dr}\tilde{y}_l(z)\right],$$
$$\qquad (A2)$$

$$\frac{E_z}{\cos\theta} = -i\frac{q}{\epsilon}e^{ikz}kr\left(\frac{1}{r^2} - \frac{1}{b^2}\right)(1 - \epsilon)$$
$$+ \sum_{l=1}^\infty \frac{\nu_l^2}{b^2}J_1\left(\frac{\nu_l r}{b}\right)x_l(z), \qquad (A3)$$

$$\frac{H_r}{\sin\theta} = -qe^{ikz}\left(\frac{1}{r^2} - \frac{1}{b^2}\right)$$
$$+ i\sum_{l=1}^{\infty}\left[\epsilon k\frac{J_1(\nu_l r/b)}{r}x_l(z) - \sigma_l\frac{dJ_1(\mu_l r/b)}{dr}\tilde{x}_l(z)\right],$$
$$\text{(A4)}$$

$$\frac{H_\theta}{\cos\theta} = qe^{ikz}\left(\frac{1}{r^2} + \frac{1}{b^2}\right)$$
$$- i\sum_{l=1}^{\infty}\left[\epsilon k\frac{dJ_1(\nu_l r/b)}{dr}x_l(z) - \sigma_l\frac{J_1(\mu_l r/b)}{r}\tilde{x}_l(z)\right],$$
$$\text{(A5)}$$

$$\frac{H_z}{\sin\theta} = i\sum_{l=1}^{\infty}\frac{\mu_l^2}{b^2}J_1\left(\frac{\mu_l r}{b}\right)\tilde{x}_l(z). \quad \text{(A6)}$$

Here $q = 2\pi N e r_0/c$, J_1 is the Bessel function of the first kind and the first order, and $0 < \nu_1 < \nu_2 < \cdots < \nu_l \cdots < \infty$ are the roots of J_1 (excluding 0) in ascending order. Likewise, $\mu_1 < \mu_2 < \cdots < \mu_l \cdots < \infty$ are the roots of $dJ_1(r)/dr$ in ascending order. The fields (A1–A6) satisfy the boundary conditions at the ideally conducting metal surface at $r = b$.

The propagation functions $x_l(z)$, $y_l(z)$ for the *TM*-modes and $\tilde{x}_l(z)$, $\tilde{y}_l(z)$ for the *TE*-modes are

$$x_l(z) = C_l^+ e^{i\lambda_l z} + C_l^- e^{-i\lambda_l z}, \quad \text{(A7)}$$

$$y_l(z) = i[C_l^+ e^{i\lambda_l z} - C_l^- e^{-i\lambda_l z}], \quad \text{(A8)}$$

$$\tilde{x}_l(z) = \tilde{C}_l^+ e^{i\sigma_l z} + \tilde{C}_l^- e^{-i\sigma_l z}, \quad \text{(A9)}$$

$$\tilde{y}_l(z) = i[\tilde{C}_l^+ e^{i\sigma_l z} - \tilde{C}_l^- e^{-i\sigma_l z}] \quad \text{(A10)}$$

where the constant complex amplitudes C_l^+, C_l^-, $\tilde{C}_l^+$, and $\tilde{C}_l^-$ are unknown and should be defined from the boundary and continuity conditions at the interface of regions with different radii. Further, the propagation constants for the *TM*- and *TE*-modes, respectively, are

$$\lambda_l = \sqrt{\epsilon k^2 - \frac{\nu_l^2}{b^2}}, \quad \text{(A11)}$$

and

$$\sigma_l = \sqrt{\epsilon k^2 - \frac{\mu_l^2}{b^2}}. \quad \text{(A12)}$$

ACKNOWLEDGMENT

REFERENCES

[1] J. W. Wang and B. W. Littmann, "Design study on quasiconstant gradient accelerating structure," SLAC Rep. AP-32, 1991.
[2] K. L. F. Bane and R. L. Gluckstern, "The transverse wakefield of a detuned X-band accelerator structure," *Part. Accel.*, vol. 42, pp. 123–169, 1994.
[3] S. A. Heifets and S. A. Kheifets, "Longitudinal electromagnetic fields in an aperiodic structures," *IEEE Trans. Microwave Theory Tech.*, vol. 42, no. 1, pp. 108–118, 1993.
[4] _____, "RF pulse transmission through an accelerating section," SLAC Note AAS-74, 1992.
[5] _____, "Study of the energy gain and the beam loading of the detuned structures with a simple model," SLAC Rep. AP-96, 1993.
[6] H. G. Beye *et al.*, "Modal field matching in tapered multicell structures," in *Proc. 15th Intern. Conf. on High Energy Accel.*, Hamburg, Germany, July 1992, and *Int. J. Mod. Phys. A*, pp. 845–847.
[7] U. Van Rienen, "Higher order mode analysis of tapered disc-loaded waveguides using the mode matching technique," *Part. Accel.*, vol. 41, pp. 173–201, 1993.
[8] W. Bruns, "Beam coupling impedance of axial symmetric structures," Technische Universitaet Berlin, private communication, 1993.
[9] T. Weiland, "Transverse beam cavity interaction, Part I: Short range forces," *Nucl. Instrum. Methods*, vol. 212, pp. 13–21, 1983.
[10] Y. H. Chin, "Advanced and applications of ABCI," LBL/Univ. of California Rep. LBL-33268/UC-414, 1993.
[11] B. Zotter and K. Bane, "Transverse resonances of periodically widened cylindrical tubes with circular cross section," SLAC Rep. PEP-308, 1979.
[12] T. Weiland, "On the computation of resonant modes in cylindrically symmetric cavities," *Nucl. Instrum. Methods*, vol. 216, pp. 329–348, 1983.
[13] S. A. Heifets and S. A. Kheifets, "Coupling impedance in modern accelerators," *Rev. Modern Phys.*, vol. 63, no. 3, pp. 631–674, 1991.
[14] W. K. H. Panofsky and W. A. Wenzel, "Some considerations concerning the transverse deflection of charged particles in radio-frequency fields," *Rev. Sci. Instr.*, vol. 27, p. 967, 1956.
[15] T. Weiland, "Comment on wake field computation in time domain," *Nucl. Instrum. Methods*, vol. 216, pp. 31–34, 1983.
[16] K. L. F. Bane, "Constructing the wake potentials from the empty cavity solutions of Maxwell's equations," *CERN/ISR-TH/80-47* (1980).
[17] K. L. F. Bane, P. B. Wilson, and T. Weiland, "Wake fields and wake field acceleration," in *Proc. Brookhaven National Lab. Accel. School*, Upton, NY, 1993, p. 975.

S. A. Kheifets, photograph and biography not available at the time of publication.

S. A. Heifets, photograph and biography not available at the time of publication.

B. Woo, photograph and biography not available at the time of publication.